

1 **Insights into characteristics and formation mechanisms of secondary organic**
2 **aerosols in Guangzhou urban area**

3 **Miaomiao Zhai^{1,3}, Ye Kuang^{1,3*}, Li Liu^{2,*}, Yao He^{1,3}, Biao Luo^{1,3}, Wanyun Xu⁴, Jiangchuan**
4 **Tao^{1,3}, Yu Zou², Fei Li^{2,5}, Changqin Yin^{2,7}, Chunhui Li², Hanbing Xu⁶, Xuejiao Deng²**

5 ¹ Institute for Environmental and Climate Research, Jinan University, Guangzhou, China.

6 ² Key Laboratory of Regional Numerical Weather Prediction, Institute of Tropical and Marine
7 Meteorology, China Meteorological Administration, Guangzhou, 510640, China

8 ³ Guangdong-Hongkong-Macau Joint Laboratory of Collaborative Innovation for Environmental
9 Quality, Guangzhou, China.

10 ⁴ State Key Laboratory of Severe Weather & Key Laboratory for Atmospheric Chemistry, Institute of
11 Atmospheric Composition, Chinese Academy of Meteorological Sciences, Beijing, 100081, China

12 ⁵ Xiamen Key Laboratory of Straits Meteorology, Xiamen Meteorological Bureau, Xiamen, 361012,
13 China

14 ⁶ Experimental Teaching Center, Sun Yat-Sen University, Guangzhou 510275, China

15 ⁷ Shanghai Key Laboratory of Meteorology and Health, Shanghai Meteorological Bureau, Shanghai
16 200030, China

17 *Correspondence to: Ye Kuang (kuangye@jnu.edu.cn) and Li Liu (liul@gd121.cn)

18
19
20
21
22
23
24
25
26
27
28
29
30
31
32
33
34
35
36
37

38 Abstract

39 Emission controls have substantially brought down aerosol pollution in China, however, aerosol
40 mass reductions have slowed down in recent years in the Pearl River Delta (PRD) region, where
41 secondary organic aerosol (SOA) formation poses a major challenge for air quality improvement. In
42 this study, we characterized the roles of SOA in haze formation in urban Guangzhou City of the PRD
43 using year-long aerosol mass spectrometer measurements for the first time and discussed possible
44 pathways of SOA formations. On average, organic aerosols (OA) contribute dominantly (50%) to non-
45 refractory submicron aerosol mass (NR-PM₁). The average mass concentration of SOA (including by
46 less and more oxidized OA, LOOA and MOOA) contributed most to NR-PM₁, reaching ~~ed~~ about 1.7
47 times that of primary organic aerosols (POA, including hydrocarbon-like and cooking-related OA) and
48 accounting for 32% of NR-PM₁, even more than sulfate (22%) and nitrate (16%). Seasonal variations
49 of NR-PM₁ revealed that haze formation mechanisms differed much among distinct seasons. Sulfate
50 mattered more than nitrate in fall, while nitrate was more important than sulfate in spring and winter,
51 with SOA contributing significantly to haze formations in all seasons. Daytime SOA formation was
52 weak in winter under low oxidant level and air relative humidity, whereas prominent daytime SOA
53 formation was observed in fall, spring and summer almost on a daily basis, suggesting ~~for~~ important
54 roles of photochemistry in SOA formations. Further analysis showed that the coordination of gas-phase
55 photochemistry and subsequent aqueous-phase reactions likely played significant roles in quick
56 daytime SOA formations. Obvious nighttime SOA formations were also frequently observed in spring,
57 fall and winter, and it was found that daytime and nighttime SOA formations together had resulted in
58 the highest SOA concentrations in these seasons and contributed substantially to severe haze
59 formations. Simultaneous increases of nitrate with SOA after sunset suggested the important roles of
60 NO₃ radical chemistry in nighttime SOA formations, and this was further confirmed by continuous
61 increase of NO⁺/NO₂⁺ fragment ratio that related to measured particulate nitrate after sunset. Findings
62 of this study have promoted our understanding ~~of~~ haze pollution characteristics of the PRD and laid
63 down future directions on investigations of SOA formation mechanisms in urban areas of southern
64 China that share similar emission sources and meteorological conditions.

65

66 1 Introduction

67 Ubiquitous submicron aerosols in the atmosphere not only deteriorate human health and visibility,
68 but also impact climate through interactions with solar radiation and clouds. Organic aerosols (OA)
69 represent one of the most important and sometimes even dominant components (~10-90%) of PM₁
70 (aerosol particles with aerodynamic diameter less than 1 μm) in urban, rural and remote areas (Zhang
71 et al., 2007; Jimenez et al., 2009). OA can either be emitted directly from emission sources or be formed
72 through atmospheric reactions of volatile organic compounds, the former is referred to as primary OA
73 (POA) and the latter is referred to as secondary OA (SOA). An increasing number of ~~studies~~~~researches~~
74 show that SOA account for a large fraction of OA worldwide (Zhang et al., 2007; Zhang et al., 2011),
75 and even dominate in some cases (Kuang et al., 2020). The implementation of strict emission reduction
76 policies has significantly improved the air quality of Pearl River Delta (PRD) region, which is a highly
77 industrialized area of China, and the annual mean concentration of PM_{2.5} (particulate matter with
78 aerodynamic diameter less than 2.5 μm) has been brought down to less than 30 μg/m³ (Xu et al., 2020).
79 However, the reduction of PM_{2.5} mass concentrations in PRD has slowed down substantially in recent
80 years, which might be related to the significant increases in the proportion of secondary aerosols (Xu
81 et al., 2020), especially for SOA. Insights into SOA formation mechanisms are important for air
82 pollution improvement.

83 SOA formation mechanisms are ~~a scientific hotspot~~ an active research area of interest in
84 atmospheric chemistry in the recent ten years since significant contributions of SOA to atmospheric
85 aerosol mass ~~have been~~~~were~~ fully recognized (Zhang et al., 2007; Jimenez et al., 2009), however quite
86 complex due to varying precursors, oxidants and formation pathways under different emission
87 characteristics and meteorological conditions. As to SOA formation pathways, SOA can be formed
88 through condensation of oxidized gas-phase organic vapors during the oxidation of volatile organic
89 compounds (VOCs), this type of formed SOA was usually referred to as gasSOA (Kuang et al., 2020).
90 SOA can also be formed in the aqueous phase through the further oxidation of dissolved VOCs which
91 are usually products of gas-phase oxidation of VOCs, this type of SOA was usually referred as aqSOA
92 (Ervens et al., 2011). ~~Both field measurements and laboratory studies are needed in investigating~~
93 ~~detailed SOA formation mechanisms in different regions with field measurements provide insights into~~
94 ~~key oxidants and formation pathways, thus information from field measurements are important for~~

95 ~~both designing laboratory experiments and targeting emission control strategies~~ Both field
96 measurements and laboratory studies are needed in investigating detailed SOA formation mechanisms
97 in different regions. Field measurements provide insights into key oxidants and formation pathways
98 under ambient conditions, thus information from field measurements are important for both designing
99 laboratory experiments and targeting emission control strategies. Aerosol mass spectrometers are
100 advanced on-line instruments that provide real time quantitative characterization of aerosol particle
101 compositions (Jayne et al., 2000;Canagaratna et al., 2007;Jimenez et al., 2003). Positive matrix
102 factorization (PMF) (Ulbrich et al., 2009) or a multilinear engine (ME-2) (Paatero, 1999;Canonaco et
103 al., 2013) can be employed to further resolve different OA factors that are associated with different
104 sources and formation mechanisms from the OA mass spectra. Using ~~these~~ these techniques, the SOA
105 sources and formation mechanisms are extensively investigated in China (Zhou et al., 2020), and many
106 studies found that aqueous reactions in aerosol water contributed substantially even dominantly to
107 SOA formations (Su et al., 2020) in haze episodes with daytime and nighttime SOA formations differ
108 much due to different meteorological conditions and oxidants (Rollins et al., 2012;Huang et al., 2021).

109 In fact, in a specific region, the compositions, sources, and evolution processes differ much among
110 seasons due to changes in emission sources and meteorological conditions (Li et al., 2015). Therefore,
111 long-term observations that cover measurements of different seasons were usually needed for
112 characterizing OA sources and SOA formation mechanisms, thereby helping to address the challenge
113 of fine particulate matter pollution mitigation. Even though aerosol mass spectrometers have been
114 widely used in China in recent years ~~and the importance of long-term measurements~~, most studies have
115 been conducted in specific periods due to its high cost and maintenance (He et al., 2011;Chen et al.,
116 2021b;Qin et al., 2017), resulting in few long-term characterizations of the mass concentrations and
117 chemical compositions of submicron particulate matter (PM₁). The design of Aerosol Chemical
118 Speciation Monitor (ACSM) has improved this problem to some extent (Ng et al., 2011;Sun et al.,
119 2015;Canonaco et al., 2021). For example, based on 2-year ACSM measurements, Sun et al. (2018)
120 investigate the distinct characteristics of PM₁ compositions among different seasons in Beijing urban
121 area and illustrated the dominant role of SOA in OA across different mass loading scenarios during all
122 seasons.

123 Guangzhou is an expansive metropolis in the highly industrialized PRD region. Using the aerosol

124 mass spectrometer measurements and source apportionment technique, Qin et al. (2017) and Huang et
125 al. (2011) reported that SOA contributed substantially to aerosol mass during autumn and winter in
126 Guangzhou. Guo et al. (2020) found that OA played a dominant role in PM₁ during winter in
127 Guangzhou, with OA source apportionment emphasized the dominance of SOA. Guo et al. (2020) also
128 suggested that gasSOA contributed predominantly to SOA formation during non-pollution periods,
129 other mechanisms such as heterogeneous and multiphase reactions played more important roles in
130 SOA formation during pollution episodes, however long-term aerosol spectrometer measurements that
131 help ~~for~~ characterizing OA sources and SOA formation mechanisms in this region remain lacking. In
132 this study, we performed a year-long continuous measurement of non-refractory submicron aerosols
133 (NR-PM₁) with an ACSM in urban Guangzhou from September 2020 to August 2021 to characterize
134 POA sources and investigate SOA formation mechanisms in different seasons.

135 **2 Experimental methods**

136 **2.1 sampling site and measurements**

137 A quadrupole-Aerosol Chemical Speciation Monitor (Q-ACSM) was deployed to continuously
138 measure nonrefractory PM₁ (NR-PM₁) species including OA, sulfate (SO₄), nitrate (NO₃), ammonium
139 (NH₄), and chloride (Cl) from September 2020 to August 2021 at an urban site located in Haizhu
140 wetland park of Guangzhou, which is surrounded by commercial streets and residential buildings,
141 however, with a distance of at least 1 km (Liu et al., 2022). Therefore, measurements at this site are
142 representative of the pollution characteristics of Guangzhou urban area. More detailed descriptions
143 about the sampling site and the ACSM measurements could be referred to Liu et al. (2022) and Ng et
144 al. (2011), respectively. An AE33 aethalometer (Drinovec et al., 2015) set up with a flow rate of 5
145 L/min was separately operated downstream of a PM_{2.5} inlet (BGI SCC 1.829) to measure aerosol
146 absorptions, from which optically equivalent black carbon (BC) mass concentrations in winter and
147 early spring were calculated. In addition, mass concentrations of PM_{2.5} and trace gases such as nitrogen
148 dioxide (NO₂), ozone (O₃), carbon monoxide (CO) and sulfur dioxide (SO₂) were acquired from the
149 publicly available datasets of the China National Environmental Monitoring network
150 (<http://www.cnemc.cn/en/>), which includes a site located within 5 km distance to our observation site.

151 Measurements of meteorological parameters such as temperature, wind speed and direction (WS and
152 WD), and relative humidity (RH) were made by an automatic weather station (Li et al., 2021). Aerosol
153 liquid water content (ALWC) was predicted with the ISORROPIA-II thermodynamic model in reverse
154 mode under metastable assumption (Guo et al., 2017) with aerosol chemical compositions measured
155 by Q-ACSM as inputs, with more details in Supplement Sect.S2.

156 2.2 Q-ACSM data analysis

157 The Q-ACSM data were processed using ACSM standard data analysis software (ACSM Local
158 1.5.10.0 Released July 6, 2015) written in Igor Pro (version 6.37). The composition-dependent
159 collection efficiency (CE) parameterization scheme proposed by Middlebrook et al. (2012) was chosen
160 to determine the mass concentrations of NR-PM₁ species which was also detailed in Liu et al. (2022).
161 Relative ionization efficiencies (RIEs) of 5.15 and 0.7 were adopted for ammonium and sulfate
162 quantifications which were calibrated using 300 nm pure NH₄NO₃ and (NH₄)₂SO₄ while the default
163 RIEs of 1.4, 1.1 and 1.3 was used for organic aerosol, nitrate and chloride, respectively. Moreover, we
164 also compared the mass concentrations of NR-PM₁ with PM_{2.5} to ensure the validity of ACSM data
165 during the whole study. As shown in Fig. S1 of the supplement, the measured NR-PM₁ correlates
166 highly with PM_{2.5} acquired from the nearest (about 5 km) Environmental Protection Agency site ($R^2 =$
167 0.71), and the average ratio of NR-PM₁/PM_{2.5} is 0.77 (± 0.36).

168 Unconstrained Positive matrix factorization (PMF) was performed on OA mass spectra of the
169 entire year-long dataset. For the two-factor solution, the POA factor ~~peaking~~ in the evening with low
170 O/C (~0.28) and an oxygenated OA (OOA) factor peaks in the afternoon with high O/C (~0.88) can
171 be well resolved (Fig.S2), demonstrating the markedly different influences of primary emissions and
172 SOA formations on diel aerosol mass concentrations. However, PMF-ACSM analysis of mass spectra
173 of OA measured by unit mass resolution instruments still faced some uncertainties to further resolve
174 potential POA or SOA components due to its rotational indeterminacy. For example, traffic-related
175 hydron-carbon like organic aerosols (HOA) was ~~uneasily~~ sometimes not well ~~to~~-separated from
176 cooking-related organic aerosols (COA) and there was also great uncertainty in distinguishing SOA
177 with different degrees of oxidations (Sun et al., 2012; Sun et al., 2013; Zhang et al., 2015). Therefore,
178 an improved source apportionment technique called Multilinear Engine (ME-2) was further used to

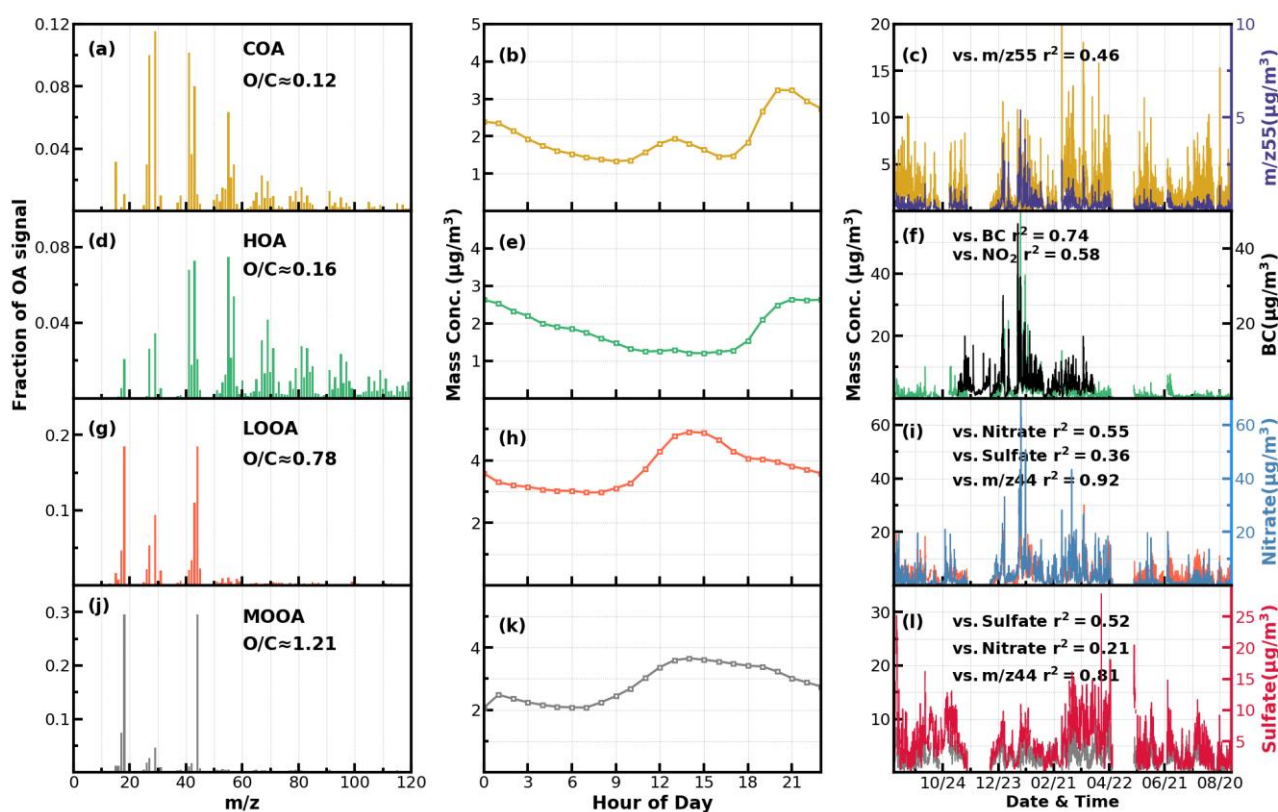


Figure 1. Mass spectral profiles, diurnal cycles and correlations with external data of COA(a-c), HOA(d-f), LOOA(g-i) and MOOA(j-l) from ME2-ACSM analysis for the entire year.

179 resolve better sources of POA and SOA (Paatero, 1999; Canonaco et al., 2013; Guo et al., 2020).
 180 Previously, both Guo et al. (2020) and Liu et al. (2022) demonstrated that during both autumn and
 181 winter seasons of Guangzhou urban areas, POA was mainly composed of HOA, (which is mostly
 182 associated with traffic emissions) and COA, while SOA could be resolved into less oxidized and
 183 more oxidized organic aerosols (LOOA and MOOA). The number selecting test using unconstrained
 184 PMF analysis (Fig.S3) also showed that four-factor solution likely be the best choice. Therefore, we
 185 had chosen 4 factors for ME-2 analysis with the a value of ME-2 rangeings from 0.1 to 0.5.
 186 Furthermore, and we constrained the HOA and COA profiles with HOA and COA profiles reported in
 187 Liu et al. (2022) as priorities considering the following three reasons: (1) The used instrument of this
 188 study is the same one of Liu et al. (2022); (2) the COA profile reported in Liu et al. (2022) was
 189 determined during the period when both COVID-19 silence-action and festival spring occurred when
 190 cooking activities grew and traffic activities almost vanished thus COA shall dominated over HOA,
 191 ~~more details about the method please refer to Liu et al. (2022)~~; (3) Resolved variations of HOA and
 192 COA are well explained by external datasets. For example, such as correlations of HOA with black

193 carbon reached 0.79. The four-factor solution using the ME-2 technique with $a=0.2$ was obtained and
 194 shown in Fig.1. The resolved HOA and COA are summed as POA, resolved LOOA and MOOA are
 195 summed as SOA, and the comparison with those resolved by the PMF is shown in Fig.2. ME-2 analysis
 196 generally reproduced both the diurnal variations as well as absolute mass concentrations of POA and
 197 SOA during different months well. To explore the consistency of resolved factors using the entire year-
 198 long dataset or only using seasonal dataset when performing ME-2 analysis, we performed individual
 199 ME-2 runs for each season. Results showed that factors resolved in each season using seasonal datasets
 200 as inputs of ME-2 are generally consistent with those resolved from year-long dataset (Fig.S4-S7).
 201 Therefore, factors resolved using the entire year-long dataset as input of ME-2 were used for further
 202 investigations and this also guaranteed consistency of factors for comparisons among seasons.

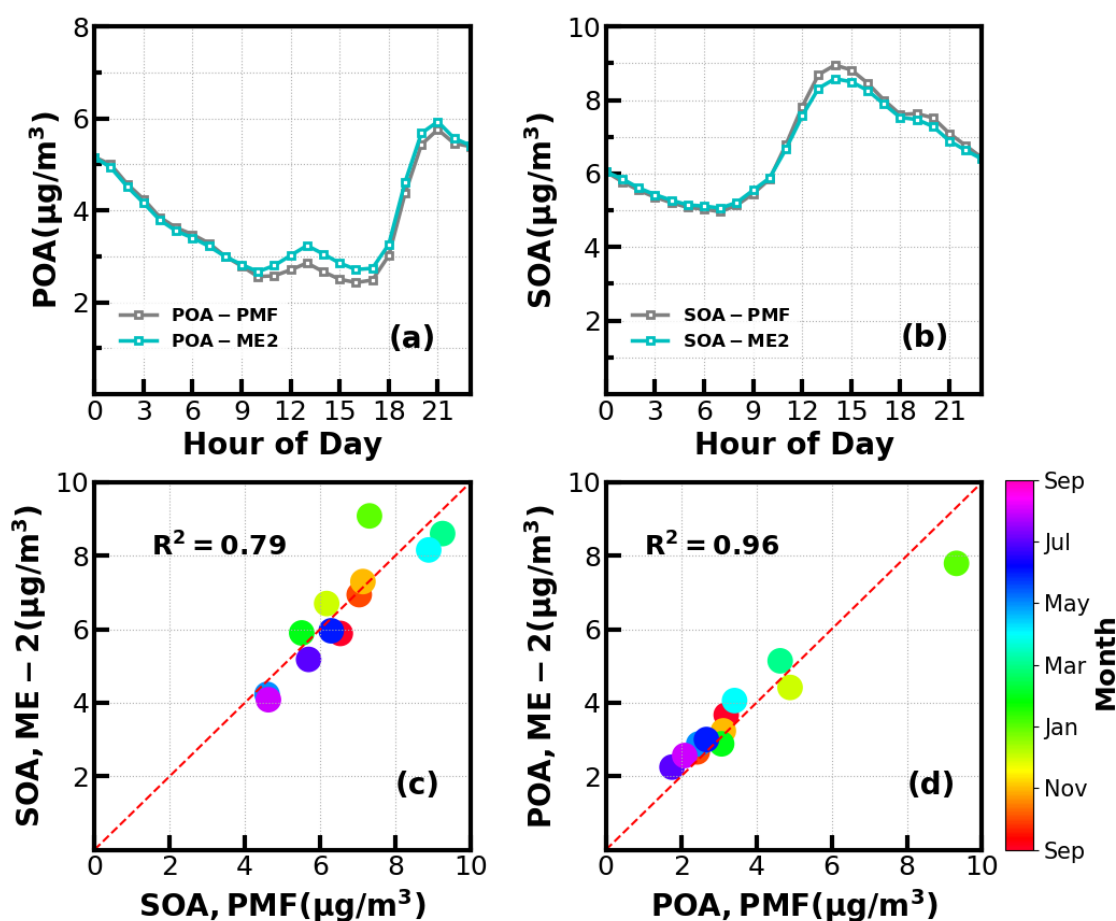


Figure 2. (a) and (b) Diurnal variations of POA and SOA concentrations from ME-2 and PMF; (c) and (d) Scatter plots between monthly average POA and SOA concentrations from ME-2 and PMF.

203 The mass spectrum of COA deconvolved in this work was characterized by a high m/z 55-to-57
 204 ratio of 2.12, which was the same with the one reported by Guo et al. (2020), and close to the m/z 55-
 205 to-57 ratio range of 2.2-2.8 reported by Mohr et al. (2012) for COA. Similar to previous studies (Guo

206 et al., 2020;Sun et al., 2013), the concentration of COA was well correlated ($R^2=0.46$) with m/z 55.
207 The O/C ratio of 0.12 for COA revealed that it was less oxidized than HOA (O/C=0.16) during the
208 whole year in Guangzhou, which was contrary to Sun et al. (2011). As shown in Fig.3, the diurnal
209 profile of COA presented two typical peaks during the entire year with a noontime peak during 13:00
210 - 14:00 LT and an evening peak during 20:00 - 21:00 LT, which were associated with noon and evening
211 cooking activities. It was noteworthy that the nighttime peak concentration of COA was very close to
212 that of noontime in summer, while the evening peak of COA was significantly higher than that of
213 noontime in other three seasons. The ratio of evening COA peak to that of the noontime was 1.7 in fall,
214 and was 1.6 in spring. In particular, the evening COA peak was nearly 4 times that of noontime in
215 winter due to the relatively insignificant noontime peak during this period, which might be associated
216 with the lock down and spring festival in winter which resulted in less noontime activities. Similar
217 conclusions could be found in Sun et al. (2018). More frequent cooking activities at night such as the
218 Chinese habit of eating midnight snacks, shallower boundary layer that inhibited diffusion of pollutants,
219 and the lower temperature at night which facilitated semi-volatile compounds from cooking emissions

220 to partition into particles resulted in the higher peak concentration at nighttime than at noon (Guo et
221 al., 2020).

222 The mass spectrum of HOA (Fig.1b) was characterized with the $C_nH_{2n-1}^+$ ($m/z = 27, 41, 55, 69$)
223 and $C_nH_{2n+1}^+$ ($m/z = 29, 43, 57, 71$) ion species. The concentration of HOA had a good correlation
224 with that of primary BC emission ($R^2=0.74$), and also correlated well with that of NO_2 ($R^2=0.58$),
225 indicating considerable impacts of traffic emissions on the HOA mass loading. As shown in Fig.3,

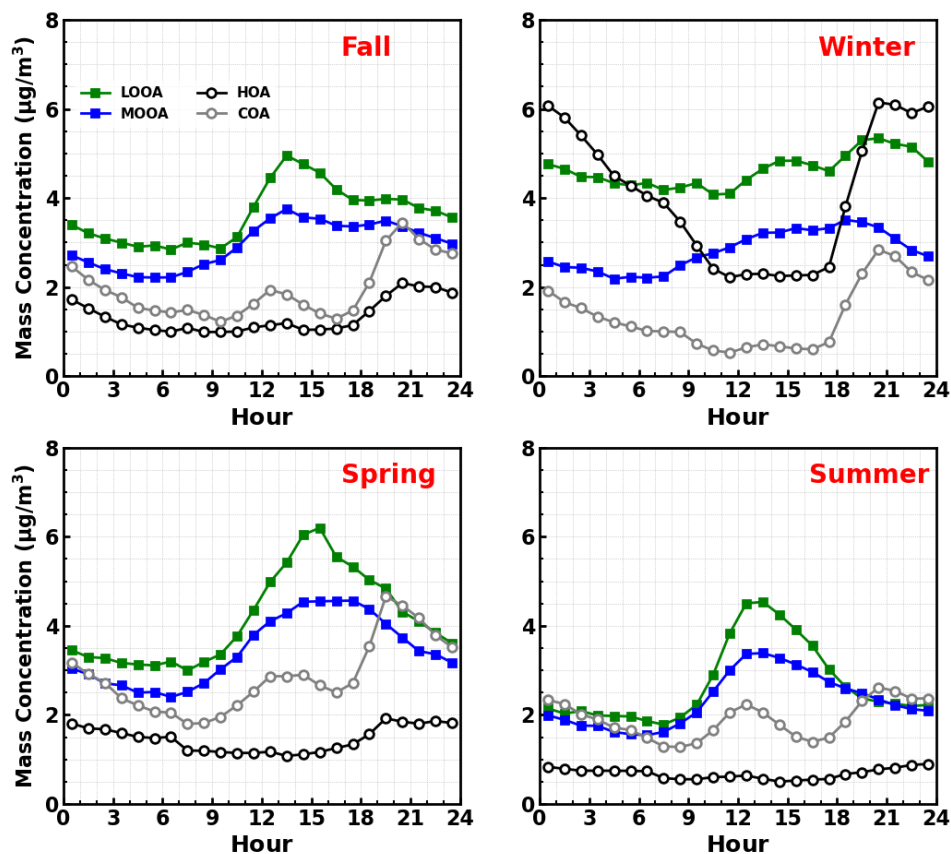


Figure 3. Diurnal profiles of HOA, COA, LOOA and MOOA in spring (March to May), summer (June to August), Fall (September to November), Winter (December to February).

226 except for summer, HOA increased significantly after sunrise especially in winter, however, began to
227 decrease in the late evening. HOA was significantly higher during nighttime than during daytime in
228 all seasons especially in winter, however, was not obvious in summer. HOA mass concentration peaks
229 around 20:00 LT were attributed to traffic emissions during the nocturnal rush hours. However, the
230 continuously high concentrations of HOA after 20:00 until 02:00 of the next day might have resulted
231 from heavy-duty vehicles with daytime traffic restrictions in Guangzhou (Guo et al., 2020; Qin et al.,
232 2017).

233 Two OOA factors were characterized with high O/C ratio, LOOA with O/C of 0.78 and MOOA

234 with O/C of 1.2, suggesting high oxidation degrees of SOA factors in Guangzhou urban area, especially
235 that of MOOA. MOOA and LOOA shared similar diurnal profiles regardless of seasons, with MOOA
236 showed higher correlations with sulfate and LOOA showed higher correlations with nitrate. MOOA
237 and LOOA increased together in fall from 09:00 LT until 14:00 LT reached a maximum of $3.7 \mu\text{g}/\text{m}^3$
238 for MOOA and $5 \mu\text{g}/\text{m}^3$ for LOOA, followed by a gradual decrease in SOA concentrations and then
239 remained relatively flat. The diurnal profiles of SOA in spring and summer were relatively similar to
240 those in fall, however, more remarkable decreases of SOA from afternoon to midnight were observed
241 in spring and summer. This is because SOA sometimes increased after sunset in autumn, which was
242 even more prominent in winter, where LOOA and MOOA would first increase for a while after sunset
243 and then begun to decrease. However, weaker daytime SOA formation was observed in winter. Note
244 that a aqSOA factor (called aqOOA in these references) was previously resolved using the aerosol
245 mass spectrometer measurements (Sun et al., 2016; Zhao et al., 2019) or time-of flight ACSM
246 measurements (Lei et al., 2021), and the factor was resolved as aqSOA because of its high fraction of
247 m/z 29 (CHO^+) and high correlation with sulfate. Both two resolved SOA factors in this study showed
248 relatively weak correlations with sulfate (Fig.1), and therefore, do not support directly ~~if they are~~
249 ~~related with~~ aqueous phase SOA formation reactions.

250 **3 Results and discussion**

251 **3.1 The largest contribution of secondary organic aerosols in NR-PM₁**

252 Time series of the meteorological parameters (including RH, WS and WD), the mass
253 concentrations of NR-PM₁ and PM_{2.5}, chemical compositions of NR-PM₁, trace gases and four
254 resolved OA factors are shown Fig.S8. It shows that emission source intensities and meteorological
255 variables changed dramatically among seasons. Hourly NR-PM₁ mass concentrations ranged from near
256 zero to $177 \mu\text{g}/\text{m}^3$ with an average of $21 \mu\text{g}/\text{m}^3$. From October to February, northerly winds prevailed
257 and average NR-PM₁ was relatively higher than that from February to September (26 vs $19 \mu\text{g}/\text{m}^3$),
258 which were associated with relatively lower boundary height during cold seasons and northern winds
259 brought polluted continental air mass. While during warm seasons of Guangzhou (March to
260 September), south-easterly wind prevailed, which brought cleaner air mass from the ocean and the

261 boundary layer height was higher due to more surface heating. Monthly variations of $PM_{2.5}$ are shown
262 in Fig.4a, $PM_{2.5}$ in summer was lowest and around $16 \mu\text{g}/\text{m}^3$ from May to August which were likely
263 associated with the prevalence of rainy conditions in summer (Fig.S9) and possibly higher boundary
264 layer height (Yang et al., 2013). January was the month with highest $PM_{2.5}$ mass concentrations with
265 an average of $49 \mu\text{g}/\text{m}^3$, which was consistent with the fact that winter usually experienced the worst
266 air pollutions due to the stagnant air conditions.

267 The average mass contributions of different components to NR- PM_{10} during the entire year and
268 among different seasons are shown in Fig.4b-4f. On average OA contributed about 50% to NR- PM_{10}
269 with the highest contribution in summer that reached near 57% and lowest contribution in spring of
270 about 47%. The second largest contributor was sulfate, which on average contributed about 22%, and
271 more than 20% in spring, summer and fall. However, the contribution of nitrate to NR- PM_{10} (23%)
272 exceeded that of sulfate (14%) and became the second major component after OA in winter, consistent
273 with the results of Guo et al. (2020) for pollution periods in winter of Guangzhou. The probability
274 distributions of mass concentrations of OA, sulfate and nitrate are shown in Fig.4g-4i. Both OA and
275 nitrate were distributed in wide ranges during winter and shared similar shape of probability
276 distribution, with OA increasing gradually from summer to winter and then reducing in the spring.
277 Sulfate shared similar magnitudes in summer and winter, and differed much from those in spring and

278 fall that had higher sulfate concentrations and varied in a wider range. Nitrate in summer and fall were
 279 relatively lower in summer and fall, however, had much higher concentrations in spring and winter.

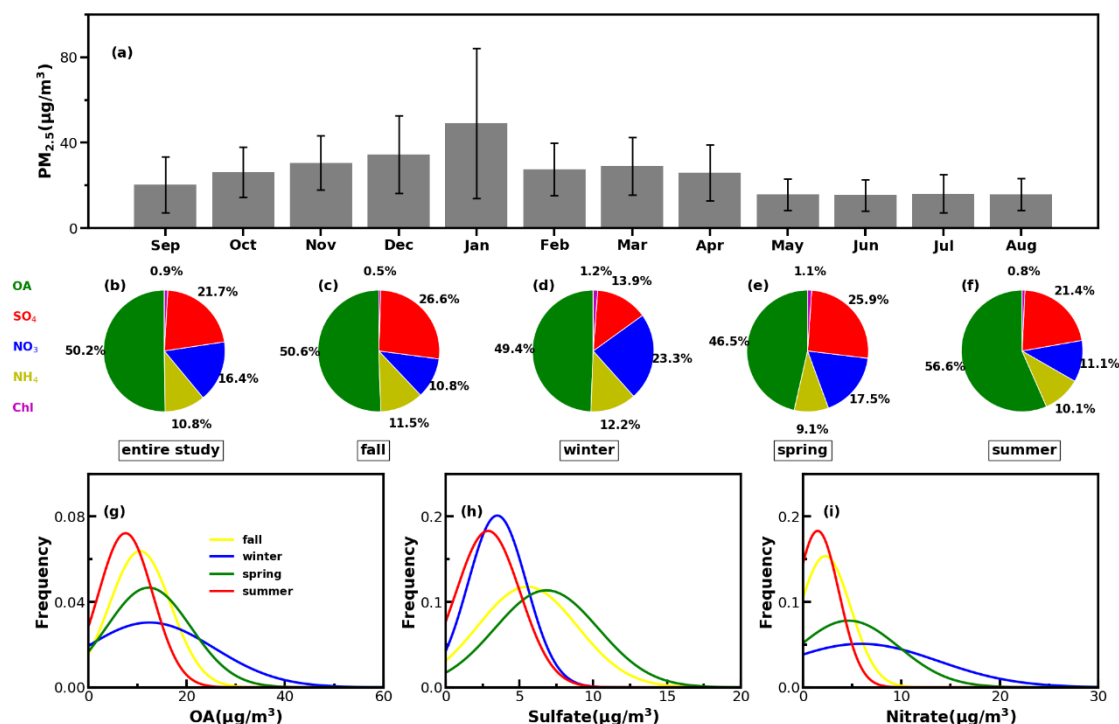


Figure 4. (a) Monthly average PM_{2.5} mass concentrations from September of 2020 to August of 2021; (b)-(f) The average mass fractions of the chemical components in NR-PM₁ of the entire year and different seasons; (g)-(i) Probability distributions of OA, sulfate (SO₄) and nitrate (NO₃) in different seasons.

280 As shown in Fig.5a, average OA concentrations of different months ranged from about 7 µg/m³
 281 to 17 µg/m³ with the peak in January and the lowest in August, and the variations of OA mass
 282 concentration in winter and spring were much larger than those in summer and autumn. Monthly
 283 variations of mass concentrations of the four resolved factors are shown in Fig.5b-5e, and contributions
 284 of the four OA factors to OA are shown in Fig.5f. In general, HOA remained lower than 2 µg/m³ in
 285 most months, however, as the cold season approached from November, the monthly average OA
 286 increased substantially from about 2 µg/m³ to near 6 µg/m³. The much lower temperature and
 287 accumulation favorable meteorological conditions likely had resulted in the substantial increase of
 288 HOA. Compared with HOA, the seasonal variations of COA were less pronounced. The monthly
 289 average concentration of COA in warm months (February to October) was higher than those in cold
 290 months (October to January). The lowest monthly average concentration of COA was about 1 µg/m³
 291 which occurred in February when the contribution of COA to OA was near its lowest of about 9%.
 292 Overall, COA contributed about 19% of OA during the whole year which was close to that of HOA

293 (18%). However, the contributions of COA and HOA to total OA differ much among seasons. The
 294 contributions of COA to OA were higher than that of HOA during warm months and lower than that
 295 of HOA in relatively cold months especially in winter. These results highlight the significant
 296 contributions of POA to OA in Guangzhou urban area, however, contributions of emission sources
 297 differed much among cold and warm seasons.

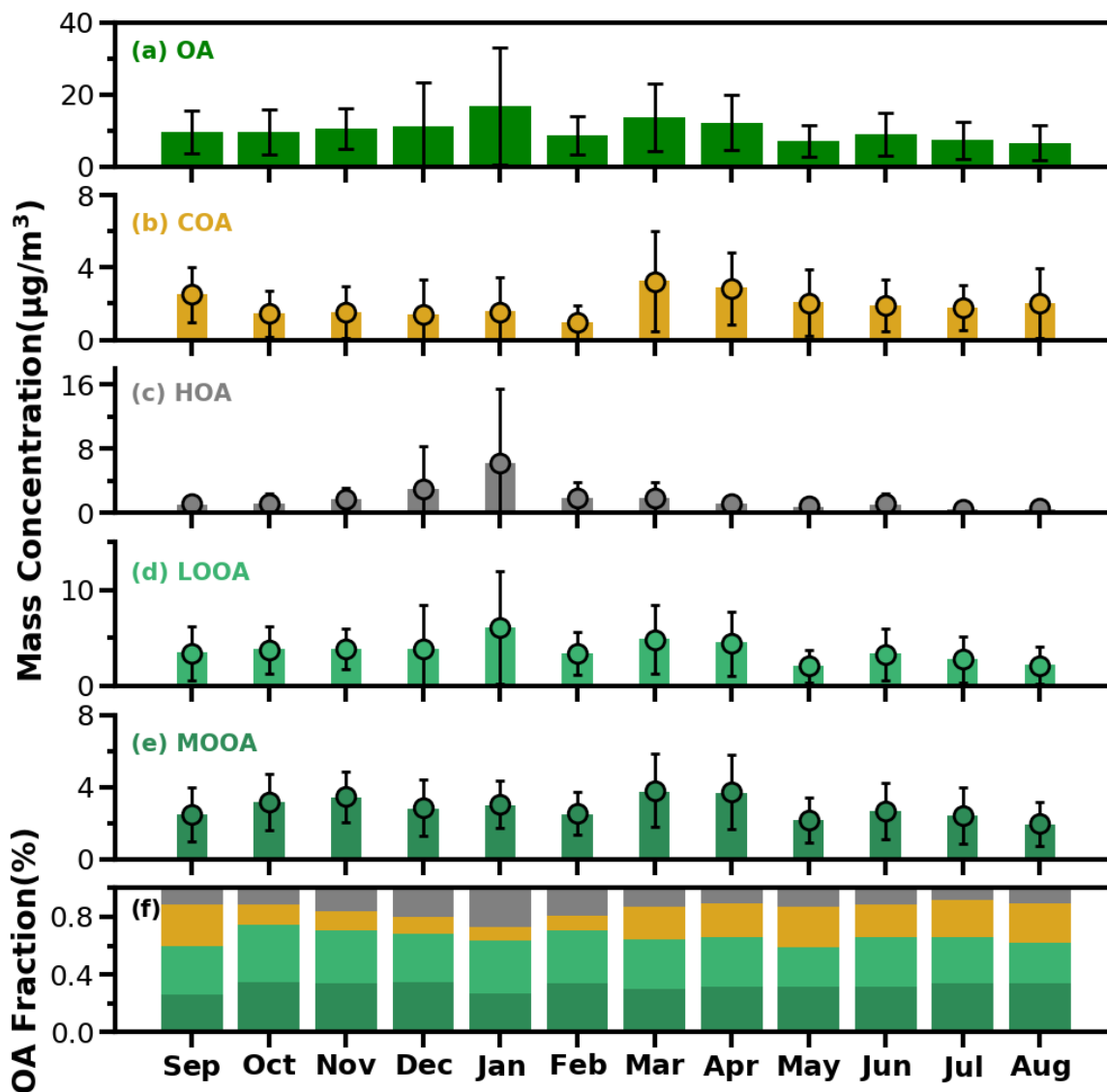


Figure 5. The bar plots of monthly average mass concentrations of OA, COA, HOA, LOOA and MOOA from (a) to (e) and mass fractions of OA factors in OA (f).

298 SOA (MOOA+LOOA) contributed more than 60% to OA in all months, reached beyond 70% in
 299 October and February, and made up on average 63% of OA in the entire year. As shown in Fig.5(e-f),
 300 LOOA exhibited stronger seasonal variations than MOOA, with monthly average mass concentrations
 301 of LOOA varying between 2.6 to 6.1 $\mu\text{g}/\text{m}^3$ and monthly average MOOA concentration ranging from

302 2 to 3.8 $\mu\text{g}/\text{m}^3$. The LOOA mass concentration peaked in the most polluted month of January,
303 suggesting that significant contributions of LOOA formation to severe haze pollution in winter. The
304 contribution of LOOA to OA ranged from 27% to 39% with an average of 34%, and the contribution
305 of MOOA to OA ranged from 26% to 35% with an average of 32%. Overall, the average mass
306 concentration of SOA was about 1.7 times that of POA for the whole year, and SOA accounted for
307 about 32% of NR-PM₁, which was higher than those of sulfate and nitrate, demonstrating the largest
308 contribution of SOA to NR-PM₁.

309 **3.2 Significant contributions of secondary organic aerosols to haze formations in all seasons**

310 Investigations on contribution variations of aerosol compositions under different aerosol pollution
311 levels are helpful for understanding mechanisms of haze formations, and results in four seasons are
312 presented in Fig.6. The chemical composition of NR-PM₁ under different pollution levels differ much
313 among seasons. In fall, as demonstrated by variations of mass concentrations of aerosol compositions
314 under different pollution levels shown in Fig.6, pollution conditions in fall were dominantly controlled
315 by secondary formations of sulfate and SOA, accumulation of primary aerosols and nitrate formation
316 had relatively smaller impacts. With respect to mass fractions variations, contributions of aerosol
317 components differed much among different pollution levels. The fraction of OA decreased rapidly from
318 67% to 50% when the mass concentration of NR-PM₁ gradually increased to 15 $\mu\text{g}/\text{m}^3$, while the
319 contribution of sulfate increased substantially from 17% to 30%, and the contribution of nitrate
320 remained relatively stable at about 10%. When NR-PM₁ further increased, OA contribution remained
321 relatively flat for NR-PM₁ below about 50 $\mu\text{g}/\text{m}^3$. Accordingly, the contribution of SO₄²⁻ decreased to
322 ~18%, and the contribution of nitrate substantially increased from ~10 % to 21%. After that, OA
323 contribution decreased rapidly to about 40% and then remained stable for NR-PM₁ >50 $\mu\text{g}/\text{m}^3$.
324 However, the contribution of sulfate began to increase, and the highest contribution could account for
325 30%, while the contribution of nitrate began to decline gradually to 12%. In addition, the SOA
326 contributed dominantly to OA (>60%) for NR-PM₁ > 15 $\mu\text{g}/\text{m}^3$ and even reached near 70% for NR-
327 PM₁ > 35 $\mu\text{g}/\text{m}^3$, suggesting the dominant role of SOA in OA accumulations in haze events during fall.

328 In winter, haze formations are mostly associated with POA accumulations, SOA and nitrate
329 formations, with nitrate formation playing the most important role, since it is also accompanied by

330 ammonium formation, while sulfate formation was weak in winter. The fraction of OA increased
 331 gradually with the increase of NR-PM₁ concentration for NR-PM₁ < 90 μg/m³ and reached the

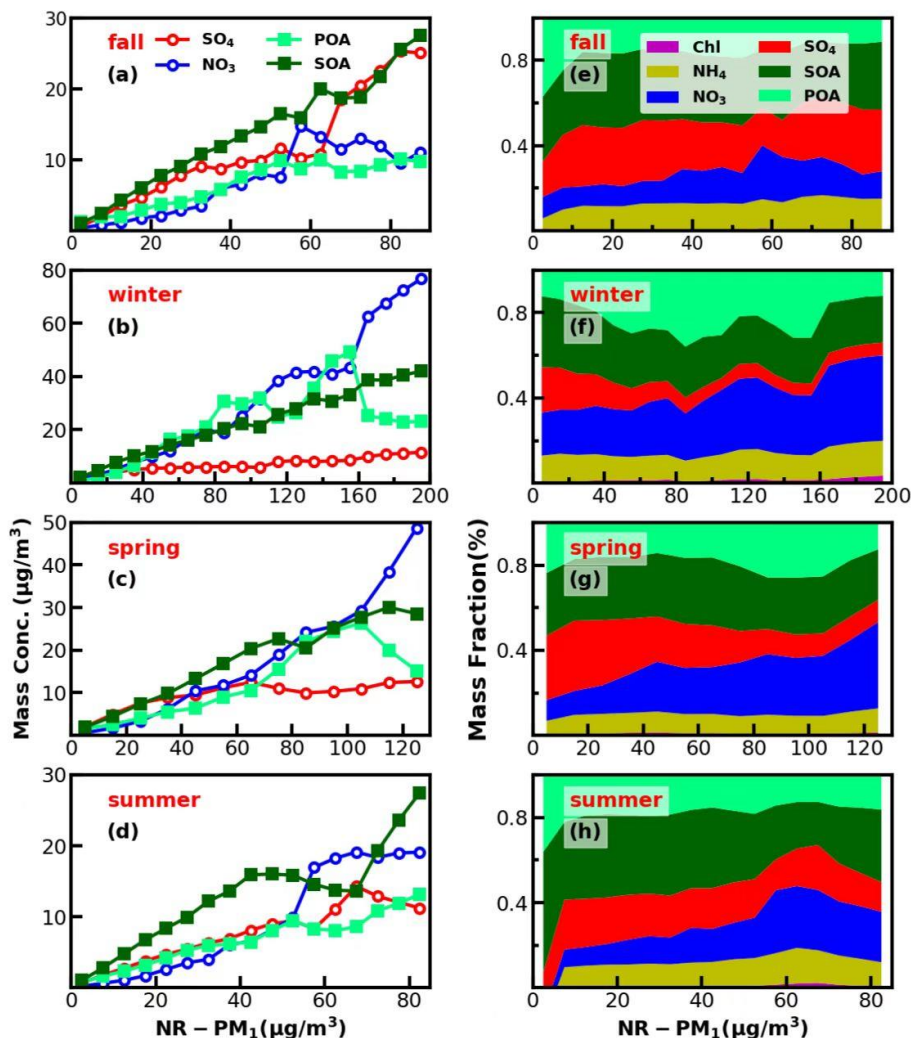


Figure 6. Left panels (a-d) show absolute mass concentration variations of aerosol compositions under different NR-PM₁ levels, right panels (e-h) show mass fractions of chemical components as a function of NR-PM₁.

332 maximum of 60%, while the contribution of nitrate also showed a small increase from 21% to 26%.
 333 Under aggravating pollution, OA contribution fluctuated, however, showed a decreasing trend from
 334 60% to ~40%. Meanwhile, the nitrate contribution showed an increasing trend from 26% to ~40%,
 335 which was similar to that of OA. Sulfate contribution decreased with the increase of NR-PM₁
 336 concentration for NR-PM₁ < 100 μg/m³ and then remained at about 6% as NR-PM₁ increases. In
 337 addition, the POA contribution increased about 25% to 50% for NR-PM₁ < 100 μg/m³. Overall, the
 338 increase of nitrate, POA and SOA together had resulted in severely polluted conditions in winter. The
 339 substantial contribution of POA to severe haze demonstrates that meteorological conditions

340 unfavorable for the pollutant diffusion together with the substantial contributions of secondary nitrate
341 and SOA formations have resulted in the most severe haze pollutions among the year. Especially, HOA
342 contribution to OA increased from 17% to 52% when NR-PM₁ concentration was less than 140 µg/m³,
343 suggesting the significant role of traffic emission accumulation during severe haze pollution, which
344 was consistent with results of Yao et al. (2020).

345 In spring, haze pollutions were mostly associated POA accumulation and secondary formations of
346 nitrate and SOA, especially that of nitrate. The contribution of OA decreased from 51% to 44% as NR-
347 PM₁ mass concentration increased when NR-PM₁ mass concentration was less than 50 µg/m³. When
348 the mass concentration of NR-PM₁ reached about 105 µg/m³, the fraction of OA reached a maximum
349 of 55%, and then decreased to about 37%. The most noticeable characteristic was the increase of nitrate
350 contribution (from 10% to 40%) and decrease of sulfate contribution (32% to 10%) as the NR-PM₁
351 increased. In summer, secondary aerosol formations contributed dominantly to haze formations, with
352 POA contribution to NR-PM₁ was about 20% in most conditions. The overall contribution of OA
353 gradually decreased from near 60% to 35% as the mass concentration of NR-PM₁ increased for NR-
354 PM₁ concentration < 60 µg/m³ which was markedly different with those in other seasons, however
355 increased to 49% as the NR-PM₁ concentration increased further. The contribution of sulfate decreased
356 from 25% to 13% and the contribution of nitrate increased from 9.0% to 31% with the increase of NR-
357 PM₁ concentration for NR-PM₁ concentration < 60 µg/m³. While the OA was dominated by SOA under
358 most conditions (about 60%).

359 Overall, haze formation mechanisms differed much among distinct seasons. Sulfate ~~was~~was
360 more significant than nitrate in fall, while nitrate ~~was more significant~~was more significant than sulfate in
361 spring and winter, however, SOA contributed significantly to haze formations in all seasons. Note that
362 seasonal variations of aerosol chemical compositions might differ much among years due to different
363 meteorological conditions and emissions. For example, the evolution of sulfate during autumn in this
364 study (Fig.S10) have remarkably different accumulation characteristics ~~from~~with those observed in
365 autumn of 2018 as shown in Fig.1 of Chen et al. (2021a). However, our conclusions about SOA playing
366 significant roles in haze formations in Guangzhou urban area during all seasons are consistent among
367 existing literature ~~Even so, SOA play significant roles in haze formations of Guangzhou urban area in~~
368 ~~all seasons hold based on results of existing literatures~~ (Zhou et al., 2020).

379 Considering the frequent co-increase of MOOA and LOOA, they were grouped together as SOA
380 for further investigations on their formation. SOA formation cases in four seasons were identified, the
381 start time and lasting hours of their occurrences, as well as associated SOA levels are shown in Fig.7.
382 Note that the identification of SOA formation cases has not considered the dilution effect of the lifting
383 daytime boundary layer height and was only based on the absolute mass concentration variations.
384 Therefore, this method has neglected some SOA formation cases that were masked by evolutions of
385 the boundary layer, and the identified cases represent active SOA formation events that overcame
386 dilution effects, which might be more suitable for further SOA formation investigations due to strong
387 SOA formation signals. It shows that in all seasons, the SOA formation happened most frequently
388 during daytime, starting in the morning and lasting about 4-8 hours. Especially, in spring, summer and
389 fall, the daytime SOA formation almost happened everyday (Fig.S5-7), even if strong daytime
390 boundary layer evolutions could be expected in these seasons due to strong surface solar heating, and
391 resulted in the afternoon SOA mass concentration peaks in these seasons (Fig.3). However, highest
392 SOA concentrations did not appear in the seasons with the most frequent morning to afternoon
393 increases. Taking SOA formation cases in spring as an example, if the SOA increase started in the
394 morning, more than 8 hours duration will result in significant higher SOA concentration. These cases
395 started in the afternoon and lasted 4-8 hours would result in highest SOA concentration in spring. The
396 SOA formation cases starting in the morning, however, only lasting within 4 hours, happened
397 frequently in summer while less in spring and fall, suggesting that the absolute SOA mass
398 concentration increase was more often stopped by strong boundary layer mixing in summer, which
399 was consistent with the solar heating characteristics. The highest SOA in fall and winter were
400 associated with the continuous increase of SOA after sunrise, suggesting that coordination of daytime
401 and nighttime SOA formation together had resulted in the highest SOA concentrations in fall and winter.

402 To dig deeper into possible mechanisms behind the active daytime SOA formations throughout
403 the year, we investigated relationships between SOA formation rates and both O₃ as well as aerosol
404 liquid water content (ALWC) for the most frequent morning to afternoon SOA increase cases. Without
405 considering the dilution effect of rising boundary layer, the daytime apparent growth rates of SOA
406 varied from 0.2 to 4.4 $\mu\text{g m}^{-3} \text{h}^{-1}$ (Fig.8). Note that the SOA growth rates was calculated on the basis
407 of observations of the first four hours for each SOA increase case to reduce impacts of boundary layer

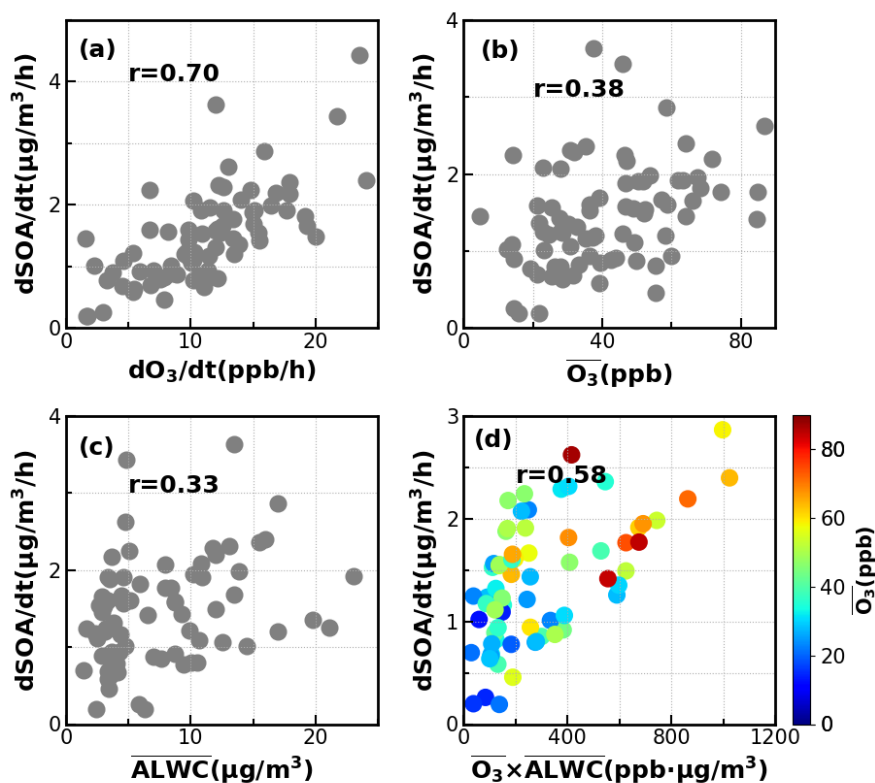


Figure 8. Relationships between SOA daytime formation rates with corresponding (a) O_3 formation rate; (b) average O_3 ; (c) average ALWC ($\mu\text{g}/\text{m}^3$) and (d) combination of averaged O_3 and averaged ALWC.

408 dilution effects. Some previous studies used variations of CO concentrations to partially correct for
 409 boundary layer dilution effects, however this method would fail in sites with strong CO emissions
 410 (Kuang et al., 2020). The SOA growth rates and were highly correlated to O_3 formation rates ($r=0.7$)
 411 as shown in Fig.8. However, this result only proved the important role of photochemistry in SOA
 412 formations. The apparent SOA growth rates showed positive but much weaker correlation with the
 413 average O_3 concentration during the period of SOA the increase ($r=0.38$), demonstrating that oxidant
 414 level was likely not the controlling factor for SOA formation, although O_3 alone did not represent the
 415 variations of oxidation levels and other sources such as HONO photolysis (Yu et al., 2022) also
 416 contribute to OH radicals and is a typical oxidant in daytime photochemistry. To investigate the
 417 possible roles of aqueous reactions in SOA formation, the relationship between apparent SOA rates
 418 and corresponding average ALWC were also investigated, and a positive but weak correlation was
 419 found ($r=0.33$). More importantly, the correlation coefficient between apparent SOA growth rates and
 420 the variable of average ALWC multiplying by average O_3 would be much higher ($r=0.58$, Fig.8d),
 421 suggesting that the coordination of gas-phase photochemistry and further aqueous reactions had likely

422 resulted in the rapid daytime SOA formations.

423 Besides the daytime SOA formation associated with photochemistry, dark transformations of
424 VOCs that involve nighttime gas-phase and aqueous phase reactions might also result in efficient SOA
425 formations. As shown in Fig.7, continuous increases of SOA were also frequently observed after sunset

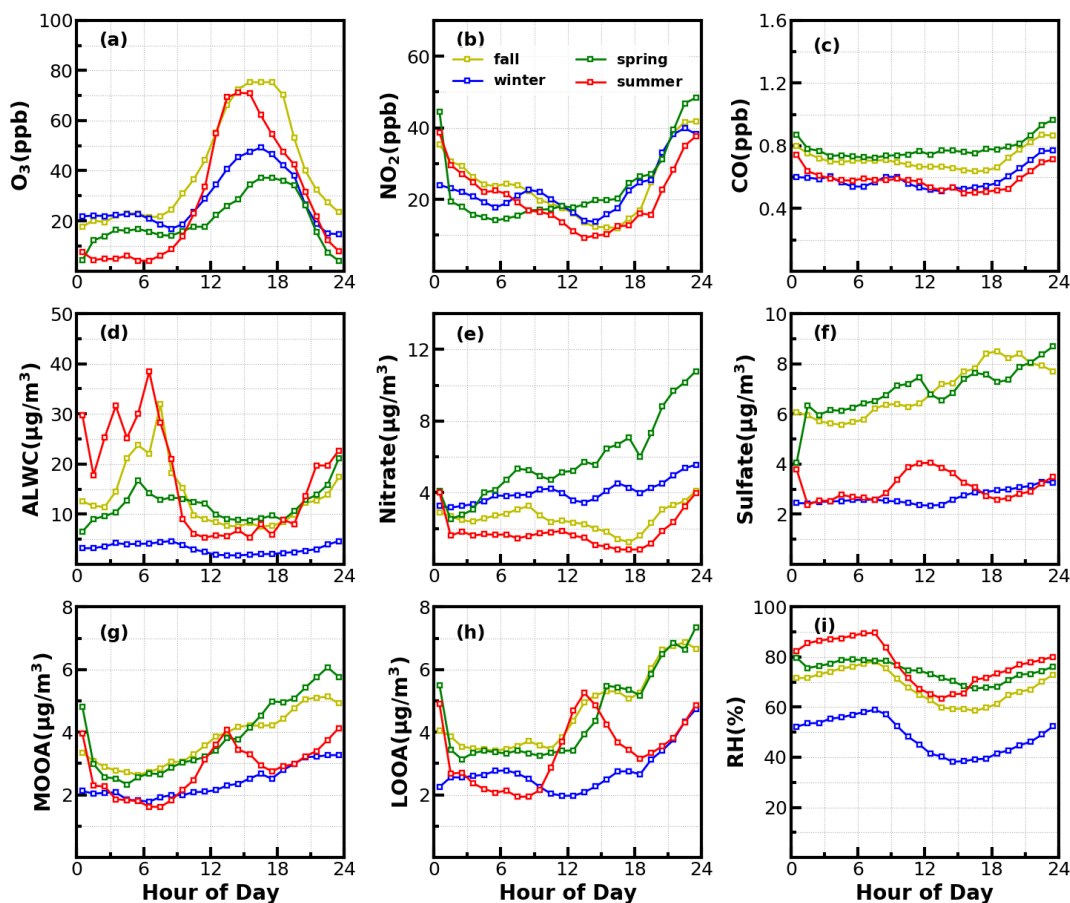


Figure 9. Average diurnal variations of (a) O₃; (b) NO₂; (c) CO; (d) ALWC; (e) nitrate; (f) sulfate; (g) MOOA; (h) LOOA and (i) RH for identified days with nighttime SOA increases.

426 in spring (17 days), fall (18 days) and winter (20 days) with sporadic occurrence in summer, and the
427 coordination of daytime and nighttime SOA formations together have resulted in the highest SOA
428 concentrations in fall and winter which were associated with severe haze pollutions as demonstrated
429 above. Average diurnal profiles of O₃, NO₂, CO, RH, ALWC, nitrate, sulfate, LOOA and MOOA for
430 cases with co-increases of LOOA and MOOA after 18:00 in different seasons are shown in Fig.9. On
431 average, SOA usually showed decreases during nighttime (Fig.3) due to transport of air mass from
432 cleaner suburban regions. The average wind speed was 1.7 m/s from 18:00 to 23:00 LT for identified
433 nighttime SOA increase cases and was obviously lower than the corresponding average wind speed of

434 2.3 m/s, suggesting the more stagnant air mass tended to favor the nighttime SOA increases. However,
 435 the nighttime 5h back trajectories shown in Fig.S11 demonstrated that the nighttime replacement of
 436 surrounding suburban cleaner air mass still prevailed, therefore the continuous increases of SOA
 437 suggested that nighttime SOA formation occurred on a regional scale. The increases of LOOA and
 438 MOOA were accompanied with obvious nitrate formation in all seasons as well as slight increases of
 439 sulfate, further indicating for regional scale nighttime secondary aerosol formations during these
 440 nighttime SOA formation events. Except for summer, continuous increase of SOA from the morning
 441 to nighttime confirmed that the coordination of daytime and nighttime SOA formations had contributed
 442 to haze formations. Number of days for daily average NR-PM₁ ranges of 0-20, 20-35, 35-45, 45-60
 443 and >60 μg/m³ were 185,85,24,10 and 7, respectively (Fig.10a). All cases with daily average NR-PM₁
 444 higher than 45 μg/m³ occurred in fall, winter and spring. The corresponding average diurnal variations

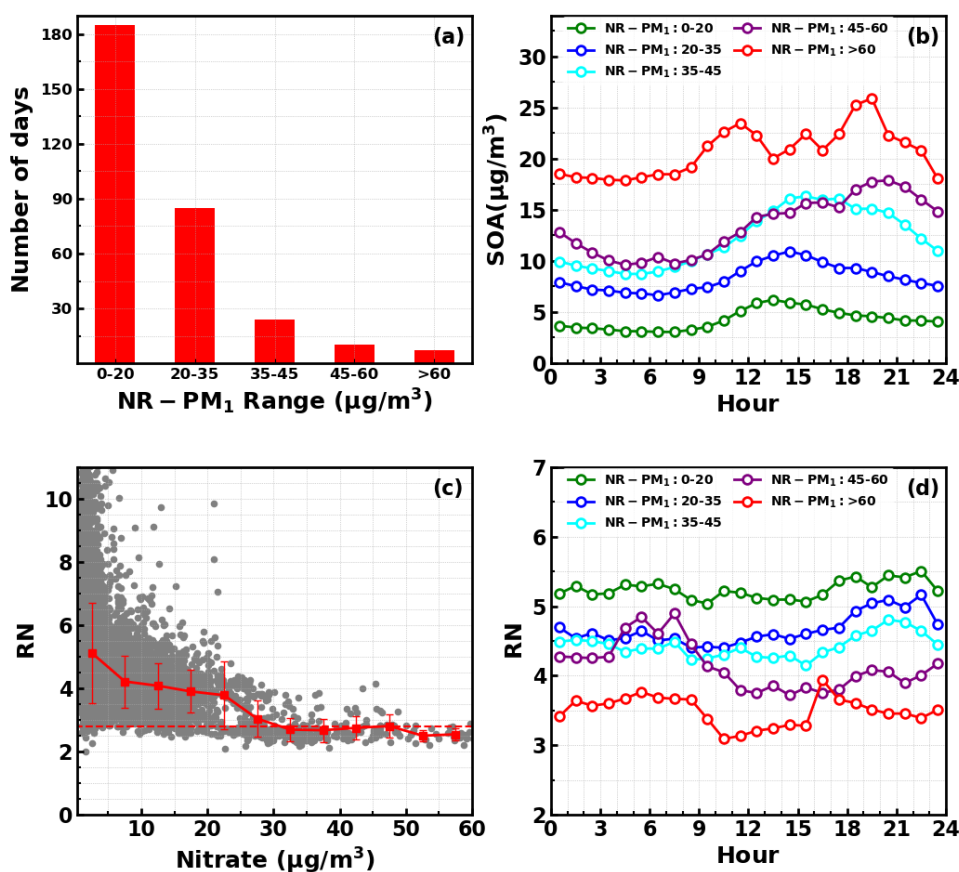


Figure 10. (a) Number of days in different daily average NR-PM₁ ranges; (b) Diurnal profiles of SOA under different NR-PM₁ ranges; (c) Variations NO⁺/NO₂⁺ (RN) as a function of measured nitrate, horizontal dashed line corresponds to RN of 2.8, red markers and bars represents averages and standard deviations; (d) Diurnal profiles of RN under different NR-PM₁ ranges.

445 of SOA for these relatively severe conditions shown in Fig.10b confirmed further that the coordination
446 of daytime and nighttime SOA formations had contributed to severe haze formations in Guangzhou
447 urban area.

448 The NO_3 radical formed through the reaction between NO_2 and O_3 is the typical nighttime oxidant.
449 Results of Rollins et al. (2012) and Kiendler-Scharr et al. (2016) revealed that NO_3 oxidation of VOCs
450 would contribute substantially to nighttime SOA increase. As shown in Fig.9a, after sunset, the O_3
451 concentration decreased quickly, however, remained substantially higher than zero, accompanied was
452 the remarkable increases of NO_2 and nitrate. In Guangzhou urban areas, nitrate can either be formed
453 through gas-phase oxidation of NO_2 by OH which forms HNO_3 and then condenses onto aerosol phase,
454 or be formed through the hydrolysis of N_2O_5 , which is formed through reactions between NO_2 and
455 NO_3 radical (Yang et al., 2022). The obvious co-increases in nitrate and SOA after sunset indicated
456 that the decrease of O_3 and increase of NO_2 consumption had supplied the NO_3 and N_2O_5 reaction
457 chains and the increase of ALWC favored the hydrolysis of N_2O_5 . This was indirectly confirmed when
458 during winter, despite relatively high concentrations of O_3 and NO_2 after sunrise compared with other
459 seasons, nitrate formation was much less prominent due to substantially lower ALWC associated with
460 lower RH. However, the quick increase of SOA still occurred after sunset despite weak daytime SOA
461 formation, suggesting that aqueous reactions might play minor roles in nighttime SOA formation that
462 involve NO_3 radical in Guangzhou urban area. The nighttime chemistry that involves NO_3 radical
463 might contribute substantially to organic nitrate formation (Ng et al., 2008; Fry et al., 2009; Rollins et
464 al., 2012) which would produce the same ions (NO^+ and NO_2^+) with inorganic nitrate due to the
465 fragmentation of nitrate functionality ($-\text{ONO}_2$) under 70 eV electron ionization in the aerosol mass
466 spectrometer measurements. However, organic nitrate has different fragmentation pattern with that of
467 inorganic nitrate with previous laboratory studies have shown that the $\text{RN}=\text{NO}^+/\text{NO}_2^+$ of organic
468 nitrate is substantially higher than that of inorganic nitrate. Farmer et al. (2010) thus proposed that the
469 RN variations can be used as an indicator of organic nitrate formations. The Q-ACSM measurements
470 with unit mass resolution cannot provide accurate measurements of RN due to the resolution limitation
471 (Allan et al., 2004), however, the resolved RN related to measured nitrate might provide qualitative
472 constraints on impacts of organic nitrates. The variations of resolved RN as a function of measured
473 nitrate are shown in Fig.10c, which shows that at high levels of nitrate when inorganic nitrate usually

474 dominates (Xu et al., 2021), the RN approaches near 2.8 which was close to the inorganic nitrate RN
475 reported in (Xu et al., 2021), and locates in the range of 1.1-3.5 of inorganic nitrate RN reported in
476 literatures (Xu et al., 2015). Diurnal variations of RN under different pollution levels shown in Fig.10d
477 reveals higher nighttime RN than daytime, and obvious continuous increase of RN after sunset can be
478 observed for relatively clean and polluted conditions (daily average NR-PM₁ of 20-35 μg/m³ to NR-
479 PM₁ of 45-60 μg/m³), suggesting active nighttime organic nitrate formations, which confirmed the
480 involvement of NO₃ radicals in nighttime SOA formations.

481 **4 Implications for future studies**

482 In this study, we highlighted the significant roles of SOA in haze formations in Guangzhou urban
483 area during the entire year and pointed out that for the most prominent and frequent daytime SOA
484 formations all the year around, both gas-phase photochemistry and aqueous reactions played
485 significant roles. Therefore, daytime SOA formation was weak in winter when oxidant level and RH
486 were low, whereas prominent SOA formations were be observed in fall, spring and summer on almost
487 daily basis. However, how gas-phase and aqueous phase reactions have coordinated to promote the
488 SOA formation, and the different contributions of gasSOA and aqSOA to SOA formations under
489 different meteorological conditions and VOCs profiles in different seasons are not clear. In addition,
490 our results suggested that the coordination of daytime and nighttime SOA formation together had
491 resulted in highest SOA concentrations in Guangzhou urban area, thus contributed significantly to
492 severe haze formation. The co-increases of nitrate and SOA after sunrise indicated the significant roles
493 of nighttime NO₃ radical chemistry in promoting haze formations. However, our understanding on
494 how nighttime chemistry evolved and contributed to secondary aerosols formations in different
495 seasons is still highly insufficient in this region. Therefore, the precursors and formation pathways of
496 daytime and nighttime SOA formations and how they coordinated to promote severe haze formations
497 need further comprehensive investigations to make targeted emission control strategies to continuously
498 improve air quality in the PRD region. Also, findings of this study have important implications on
499 future investigations of SOA formation mechanisms in urban areas of southern China that share similar
500 emission sources and meteorological conditions.

501

502 **Data availability.** All data needed are presented in time series of Figures and supplementary Figures,
503 raw datasets of this study are available from the corresponding author Li Liu (liul@gd121.cn) upon
504 request.

505

506 **Competing interests.** The authors declare that they have no conflict of interest.

507

508 **Author Contributions.** YK and LL designed the aerosol experiments. YK conceived and led this
509 research. MMZ and YK wrote the manuscript. MMZ and LL conducted the long-term Q-ACSM
510 measurements. MMZ and YH performed the PMF analysis. HBX, CY, YZ and FL helped maintain and
511 calibrating the Q-ACSM. CL provided meteorological datasets, BL performed the AE33 measurements
512 and post data processing. XJD obtained funding for the continuous aerosol measurements. JCT and
513 WYX provided insights into data analysis, and all authors contributed to revisions of this paper.

514

515

516 **Acknowledgments**

517 This work is supported by the Guangdong Provincial Key Research and Development Program
518 (2020B1111360003); National Natural Science Foundation of China (42175083 and 42105092);
519 Guangdong Basic and Applied Basic Research Foundation (2019A1515110791 and
520 2019A1515011808); National Key Research and Development Program of China (2019YFCO214605);
521 Science and Technology Innovation Team Plan of Guangdong Meteorological Bureau
522 (GRMCTD202003). The Special Fund Project for Science and Technology Innovation Strategy of
523 Guangdong Province (Grant No.2019B121205004).

524

525 **References**

526 Allan, J. D., Delia, A. E., Coe, H., Bower, K. N., Alfarra, M. R., Jimenez, J. L., Middlebrook, A. M., Drewnick, F., Onasch,
527 T. B., Canagaratna, M. R., Jayne, J. T., and Worsnop, D. R.: A generalised method for the extraction of chemically
528 resolved mass spectra from Aerodyne aerosol mass spectrometer data, *Journal of Aerosol Science*, 35, 909-922,
529 <https://doi.org/10.1016/j.jaerosci.2004.02.007>, 2004.

530 Canagaratna, M. R., Jayne, J. T., Jimenez, J. L., Allan, J. D., Alfarra, M. R., Zhang, Q., Onasch, T. B., Drewnick, F., Coe,
531 H., Middlebrook, A., Delia, A., Williams, L. R., Trimborn, A. M., Northway, M. J., DeCarlo, P. F., Kolb, C. E., Davidovits,
532 P., and Worsnop, D. R.: Chemical and microphysical characterization of ambient aerosols with the aerodyne aerosol
533 mass spectrometer, *Mass Spectrom Rev*, 26, 185–222, 10.1002/mas.20115, 2007.

534 Canonaco, F., Crippa, M., Slowik, J. G., Baltensperger, U., and Prevot, A. S. H.: SoFi, an IGOR-based interface for the
535 efficient use of the generalized multilinear engine (ME-2) for the source apportionment: ME-2 application to
536 aerosol mass spectrometer data, *Atmos. Meas. Tech.*, 6, 3649–3661, 10.5194/amt-6-3649-2013, 2013.

537 Canonaco, F., Tobler, A., Chen, G., Sosedova, Y., Slowik, J. G., Bozzetti, C., Daellenbach, K. R., El Haddad, I., Crippa,
538 M., Huang, R. J., Furger, M., Baltensperger, U., and Prévôt, A. S. H.: A new method for long-term source
539 apportionment with time-dependent factor profiles and uncertainty assessment using SoFi Pro: application to 1
540 year of organic aerosol data, *Atmos. Meas. Tech.*, 14, 923–943, 10.5194/amt-14-923-2021, 2021.

541 Chen, W., Ye, Y., Hu, W., Zhou, H., Pan, T., Wang, Y., Song, W., Song, Q., Ye, C., Wang, C., Wang, B., Huang, S., Yuan,
542 B., Zhu, M., Lian, X., Zhang, G., Bi, X., Jiang, F., Liu, J., Canonaco, F., Prevot, A. S. H., Shao, M., and Wang, X.: Real-
543 Time Characterization of Aerosol Compositions, Sources, and Aging Processes in Guangzhou During PRIDE-GBA
544 2018 Campaign, *Journal of Geophysical Research: Atmospheres*, 126, e2021JD035114,
545 <https://doi.org/10.1029/2021JD035114>, 2021a.

546 Chen, W., Ye, Y. Q., Hu, W. W., Zhou, H. S., Pan, T. L., Wang, Y. K., Song, W., Song, Q. C., Ye, C. S., Wang, C. M.,
547 Wang, B. L., Huang, S., Yuan, B., Zhu, M., Lian, X. F., Zhang, G. H., Bi, X. H., Jiang, F., Liu, J. W., Canonaco, F., Prevot,
548 A. S. H., Shao, M., and Wang, X. M.: Real-Time Characterization of Aerosol Compositions, Sources, and Aging
549 Processes in Guangzhou During PRIDE-GBA 2018 Campaign, *J Geophys Res-Atmos*, 126, ARTN e2021JD035114
550 10.1029/2021JD035114, 2021b.

551 Drinovec, L., Močnik, G., Zotter, P., Prévôt, A. S. H., Ruckstuhl, C., Coz, E., Rupakheti, M., Sciare, J., Müller, T.,
552 Wiedensohler, A., and Hansen, A. D. A.: The "dual-spot" Aethalometer: an improved measurement of aerosol black
553 carbon with real-time loading compensation, *Atmospheric Measurement Techniques*, 8, 1965–1979, 10.5194/amt-
554 8-1965-2015, 2015.

555 Ervens, B., Turpin, B. J., and Weber, R. J.: Secondary organic aerosol formation in cloud droplets and aqueous
556 particles (aqSOA): a review of laboratory, field and model studies, *Atmos. Chem. Phys.*, 11, 11069–11102,
557 10.5194/acp-11-11069-2011, 2011.

558 Farmer, D. K., Matsunaga, A., Docherty, K. S., Surratt, J. D., Seinfeld, J. H., Ziemann, P. J., and Jimenez, J. L.: Response
559 of an aerosol mass spectrometer to organonitrates and organosulfates and implications for atmospheric chemistry,
560 *Proceedings of the National Academy of Sciences*, 107, 6670–6675, doi:10.1073/pnas.0912340107, 2010.

561 Fry, J. L., Kiendler-Scharr, A., Rollins, A. W., Wooldridge, P. J., Brown, S. S., Fuchs, H., Dubé, W., Mensah, A., dal Maso,
562 M., Tillmann, R., Dorn, H. P., Brauers, T., and Cohen, R. C.: Organic nitrate and secondary organic aerosol yield from
563 NO₃ oxidation of β-pinene evaluated using a gas-phase kinetics/aerosol partitioning model, *Atmos.*
564 *Chem. Phys.*, 9, 1431–1449, 10.5194/acp-9-1431-2009, 2009.

565 Guo, H., Liu, J., Froyd, K. D., Roberts, J. M., Veres, P. R., Hayes, P. L., Jimenez, J. L., Nenes, A., and Weber, R. J.: Fine
566 particle pH and gas-particle phase partitioning of inorganic species in Pasadena, California, during the 2010 CalNex
567 campaign, *Atmospheric Chemistry and Physics*, 17, 5703–5719, 10.5194/acp-17-5703-2017, 2017.

568 Guo, J. C., Zhou, S. Z., Cai, M. F., Zhao, J., Song, W., Zhao, W. X., Hu, W. W., Sun, Y. L., He, Y., Yang, C. Q., Xu, X. Z.,
569 Zhang, Z. S., Cheng, P., Fan, Q., Hang, J., Fan, S. J., Wang, X. M., and Wang, X. M.: Characterization of submicron
570 particles by time-of-flight aerosol chemical speciation monitor (ToF-ACSM) during wintertime: aerosol
571 composition, sources, and chemical processes in Guangzhou, China, *Atmospheric Chemistry and Physics*, 20, 7595–
572 7615, 10.5194/acp-20-7595-2020, 2020.

573 He, L. Y., Huang, X. F., Xue, L., Hu, M., Lin, Y., Zheng, J., Zhang, R. Y., and Zhang, Y. H.: Submicron aerosol analysis

574 and organic source apportionment in an urban atmosphere in Pearl River Delta of China using high-resolution
575 aerosol mass spectrometry, *J Geophys Res-Atmos*, 116, Artn D12304
576 10.1029/2010jd014566, 2011.

577 Huang, X., Ding, A., Gao, J., Zheng, B., Zhou, D., Qi, X., Tang, R., Wang, J., Ren, C., Nie, W., Chi, X., Xu, Z., Chen, L.,
578 Li, Y., Che, F., Pang, N., Wang, H., Tong, D., Qin, W., Cheng, W., Liu, W., Fu, Q., Liu, B., Chai, F., Davis, S. J., Zhang, Q.,
579 and He, K.: Enhanced secondary pollution offset reduction of primary emissions during COVID-19 lockdown in
580 China, *National Science Review*, 8, nwa137, 10.1093/nsr/nwa137, 2021.

581 Huang, X. F., He, L. Y., Hu, M., Canagaratna, M. R., Kroll, J. H., Ng, N. L., Zhang, Y. H., Lin, Y., Xue, L., Sun, T. L., Liu, X.
582 G., Shao, M., Jayne, J. T., and Worsnop, D. R.: Characterization of submicron aerosols at a rural site in Pearl River
583 Delta of China using an Aerodyne High-Resolution Aerosol Mass Spectrometer, *Atmospheric Chemistry and Physics*,
584 11, 1865-1877, 10.5194/acp-11-1865-2011, 2011.

585 Jayne, J. T., Leard, D. C., Zhang, X. F., Davidovits, P., Smith, K. A., Kolb, C. E., and Worsnop, D. R.: Development of an
586 aerosol mass spectrometer for size and composition analysis of submicron particles, *Aerosol Science and*
587 *Technology*, 33, 49-70, Doi 10.1080/027868200410840, 2000.

588 Jimenez, J. L., Jayne, J. T., Shi, Q., Kolb, C. E., Worsnop, D. R., Yourshaw, I., Seinfeld, J. H., Flagan, R. C., Zhang, X. F.,
589 Smith, K. A., Morris, J. W., and Davidovits, P.: Ambient aerosol sampling using the Aerodyne Aerosol Mass
590 Spectrometer, *J Geophys Res-Atmos*, 108, Artn 8425
591 10.1029/2001jd001213, 2003.

592 Jimenez, J. L., Canagaratna, M. R., Donahue, N. M., Prevot, A. S. H., Zhang, Q., Kroll, J. H., DeCarlo, P. F., Allan, J. D.,
593 Coe, H., Ng, N. L., Aiken, A. C., Docherty, K. S., Ulbrich, I. M., Grieshop, A. P., Robinson, A. L., Duplissy, J., Smith, J. D.,
594 Wilson, K. R., Lanz, V. A., Hueglin, C., Sun, Y. L., Tian, J., Laaksonen, A., Raatikainen, T., Rautiainen, J., Vaattovaara, P.,
595 Ehn, M., Kulmala, M., Tomlinson, J. M., Collins, D. R., Cubison, M. J., Dunlea, J., Huffman, J. A., Onasch, T. B., Alfarra,
596 M. R., Williams, P. I., Bower, K., Kondo, Y., Schneider, J., Drewnick, F., Borrmann, S., Weimer, S., Demerjian, K., Salcedo,
597 D., Cottrell, L., Griffin, R., Takami, A., Miyoshi, T., Hatakeyama, S., Shimono, A., Sun, J. Y., Zhang, Y. M., Dzepina, K.,
598 Kimmel, J. R., Sueper, D., Jayne, J. T., Herndon, S. C., Trimborn, A. M., Williams, L. R., Wood, E. C., Middlebrook, A.
599 M., Kolb, C. E., Baltensperger, U., and Worsnop, D. R.: Evolution of Organic Aerosols in the Atmosphere, *Science*,
600 326, 1525-1529, 10.1126/science.1180353, 2009.

601 Kiendler-Scharr, A., Mensah, A. A., Friese, E., Topping, D., Nemitz, E., Prevot, A. S. H., Äijälä, M., Allan, J., Canonaco,
602 F., Canagaratna, M., Carbone, S., Crippa, M., Dall'Osto, M., Day, D. A., De Carlo, P., Di Marco, C. F., Elbern, H., Eriksson,
603 A., Freney, E., Hao, L., Herrmann, H., Hildebrandt, L., Hillamo, R., Jimenez, J. L., Laaksonen, A., McFiggans, G., Mohr,
604 C., O'Dowd, C., Otjes, R., Ovadnevaite, J., Pandis, S. N., Poulain, L., Schlag, P., Sellegri, K., Swietlicki, E., Tiitta, P.,
605 Vermeulen, A., Wahner, A., Worsnop, D., and Wu, H.-C.: Ubiquity of organic nitrates from nighttime chemistry in
606 the European submicron aerosol, *Geophysical Research Letters*, 43, 7735-7744, 10.1002/2016gl069239, 2016.

607 Kuang, Y., He, Y., Xu, W., Yuan, B., Zhang, G., Ma, Z., Wu, C., Wang, C., Wang, S., Zhang, S., Tao, J., Ma, N., Su, H.,
608 Cheng, Y., Shao, M., and Sun, Y.: Photochemical Aqueous-Phase Reactions Induce Rapid Daytime Formation of
609 Oxygenated Organic Aerosol on the North China Plain, *Environmental science & technology*, 54, 3849-3860,
610 10.1021/acs.est.9b06836, 2020.

611 Lei, L., Sun, Y., Ouyang, B., Qiu, Y., Xie, C., Tang, G., Zhou, W., He, Y., Wang, Q., Cheng, X., Fu, P., and Wang, Z.:
612 Vertical Distributions of Primary and Secondary Aerosols in Urban Boundary Layer: Insights into Sources, Chemistry,
613 and Interaction with Meteorology, *Environmental science & technology*, 55, 4542-4552, 10.1021/acs.est.1c00479,
614 2021.

615 Li, Y. J., Lee, B. P., Su, L., Fung, J. C. H., and Chan, C. K.: Seasonal characteristics of fine particulate matter (PM) based
616 on high-resolution time-of-flight aerosol mass spectrometric (HR-ToF-AMS) measurements at the HKUST
617 Supersite in Hong Kong, *Atmos. Chem. Phys.*, 15, 37-53, 10.5194/acp-15-37-2015, 2015.

618 Li, Z., Lei, L., Li, Y., Chen, C., Wang, Q., Zhou, W., Sun, J., Xie, C., and Sun, Y.: Aerosol characterization in a city in
619 central China plain and implications for emission control, *J Environ Sci (China)*, 104, 242-252,
620 10.1016/j.jes.2020.11.015, 2021.

621 Liu, L., Kuang, Y., Zhai, M., Xue, B., He, Y., Tao, J., Luo, B., Xu, W., Tao, J., Yin, C., Li, F., Xu, H., Deng, T., Deng, X., Tan,
622 H., and Shao, M.: Strong light scattering of highly oxygenated organic aerosols impacts significantly on visibility
623 degradation, *Atmos. Chem. Phys.*, 22, 7713-7726, 10.5194/acp-22-7713-2022, 2022.

624 Middlebrook, A. M., Bahreini, R., Jimenez, J. L., and Canagaratna, M. R.: Evaluation of Composition-Dependent
625 Collection Efficiencies for the Aerodyne Aerosol Mass Spectrometer using Field Data, *Aerosol Science and
626 Technology*, 46, 258-271, 10.1080/02786826.2011.620041, 2012.

627 Mohr, C., DeCarlo, P. F., Heringa, M. F., Chirico, R., Slowik, J. G., Richter, R., Reche, C., Alastuey, A., Querol, X., Seco,
628 R., Penuelas, J., Jimenez, J. L., Crippa, M., Zimmermann, R., Baltensperger, U., and Prevot, A. S. H.: Identification and
629 quantification of organic aerosol from cooking and other sources in Barcelona using aerosol mass spectrometer
630 data, *Atmospheric Chemistry and Physics*, 12, 1649-1665, 10.5194/acp-12-1649-2012, 2012.

631 Ng, N. L., Kwan, A. J., Surratt, J. D., Chan, A. W. H., Chhabra, P. S., Sorooshian, A., Pye, H. O. T., Crouse, J. D.,
632 Wennberg, P. O., Flagan, R. C., and Seinfeld, J. H.: Secondary organic aerosol (SOA) formation from reaction of
633 isoprene with nitrate radicals (NO_3), *Atmos. Chem. Phys.*, 8, 4117-4140, 10.5194/acp-8-4117-2008,
634 2008.

635 Ng, N. L., Herndon, S. C., Trimborn, A., Canagaratna, M. R., Croteau, P. L., Onasch, T. B., Sueper, D., Worsnop, D. R.,
636 Zhang, Q., Sun, Y. L., and Jayne, J. T.: An Aerosol Chemical Speciation Monitor (ACSM) for Routine Monitoring of
637 the Composition and Mass Concentrations of Ambient Aerosol, *Aerosol Science and Technology*, 45, 780-794, Pii
638 934555189
639 10.1080/02786826.2011.560211, 2011.

640 Paatero, P.: The Multilinear Engine—A Table-Driven, Least Squares Program for Solving Multilinear Problems,
641 Including then-Way Parallel Factor Analysis Model, *Journal of Computational and Graphical Statistics*, 8, 854-888,
642 10.1080/10618600.1999.10474853, 1999.

643 Qin, Y. M., Tan, H. B., Li, Y. J., Schurman, M. I., Li, F., Canonaco, F., Prevot, A. S. H., and Chan, C. K.: Impacts of traffic
644 emissions on atmospheric particulate nitrate and organics at a downwind site on the periphery of Guangzhou,
645 China, *Atmospheric Chemistry and Physics*, 17, 10245-10258, 10.5194/acp-17-10245-2017, 2017.

646 Rollins, A. W., Browne, E. C., Min, K. E., Pusede, S. E., Wooldridge, P. J., Gentner, D. R., Goldstein, A. H., Liu, S., Day,
647 D. A., Russell, L. M., and Cohen, R. C.: Evidence for NO_x Control over
648 Nighttime SOA Formation, *Science*, 337, 1210, 10.1126/science.1221520, 2012.

649 Su, H., Cheng, Y., and Pöschl, U.: New Multiphase Chemical Processes Influencing Atmospheric Aerosols, *Air Quality,
650 and Climate in the Anthropocene*, *Accounts of chemical research*, 53, 2034-2043, 10.1021/acs.accounts.0c00246,
651 2020.

652 Sun, Y., Du, W., Fu, P., Wang, Q., Li, J., Ge, X., Zhang, Q., Zhu, C., Ren, L., Xu, W., Zhao, J., Han, T., Worsnop, D. R.,
653 and Wang, Z.: Primary and secondary aerosols in Beijing in winter: sources, variations and processes, *Atmos. Chem.
654 Phys.*, 16, 8309-8329, 10.5194/acp-16-8309-2016, 2016.

655 Sun, Y. L., Zhang, Q., Schwab, J. J., Demerjian, K. L., Chen, W. N., Bae, M. S., Hung, H. M., Hogrefe, O., Frank, B.,
656 Rattigan, O. V., and Lin, Y. C.: Characterization of the sources and processes of organic and inorganic aerosols in
657 New York city with a high-resolution time-of-flight aerosol mass spectrometer, *Atmospheric Chemistry and Physics*,
658 11, 1581-1602, 10.5194/acp-11-1581-2011, 2011.

659 Sun, Y. L., Wang, Z. F., Dong, H. B., Yang, T., Li, J., Pan, X. L., Chen, P., and Jayne, J. T.: Characterization of summer
660 organic and inorganic aerosols in Beijing, China with an Aerosol Chemical Speciation Monitor, *Atmos. Environ.*, 51,
661 250-259, 10.1016/j.atmosenv.2012.01.013, 2012.

662 Sun, Y. L., Wang, Z. F., Fu, P. Q., Yang, T., Jiang, Q., Dong, H. B., Li, J., and Jia, J. J.: Aerosol composition, sources and
663 processes during wintertime in Beijing, China, *Atmospheric Chemistry and Physics*, 13, 4577–4592, 10.5194/acp-
664 13-4577-2013, 2013.

665 Sun, Y. L., Wang, Z. F., Du, W., Zhang, Q., Wang, Q. Q., Fu, P. Q., Pan, X. L., Li, J., Jayne, J., and Worsnop, D. R.: Long-
666 term real-time measurements of aerosol particle composition in Beijing, China: seasonal variations, meteorological
667 effects, and source analysis, *Atmospheric Chemistry and Physics*, 15, 10149–10165, 10.5194/acp-15-10149-2015,
668 2015.

669 Sun, Y. L., Xu, W. Q., Zhang, Q., Jiang, Q., Canonaco, F., Preevot, A. S. H., Fu, P. Q., Li, J., Jayne, J., Worsnop, D. R.,
670 and Wang, Z. F.: Source apportionment of organic aerosol from 2-year highly time-resolved measurements by an
671 aerosol chemical speciation monitor in Beijing, China, *Atmospheric Chemistry and Physics*, 18, 8469–8489,
672 10.5194/acp-18-8469-2018, 2018.

673 Ulbrich, I. M., Canagaratna, M. R., Zhang, Q., Worsnop, D. R., and Jimenez, J. L.: Interpretation of organic
674 components from Positive Matrix Factorization of aerosol mass spectrometric data, *Atmospheric Chemistry and
675 Physics*, 9, 2891–2918, 10.5194/acp-9-2891-2009, 2009.

676 Xu, L., Suresh, S., Guo, H., Weber, R. J., and Ng, N. L.: Aerosol characterization over the southeastern United States
677 using high-resolution aerosol mass spectrometry: spatial and seasonal variation of aerosol composition and sources
678 with a focus on organic nitrates, *Atmos. Chem. Phys.*, 15, 7307–7336, 10.5194/acp-15-7307-2015, 2015.

679 Xu, W., Kuang, Y., Bian, Y., Liu, L., Li, F., Wang, Y., Xue, B., Luo, B., Huang, S., Yuan, B., Zhao, P., and Shao, M.: Current
680 Challenges in Visibility Improvement in Southern China, *Environmental Science & Technology Letters*, 7, 395–401,
681 10.1021/acs.estlett.0c00274, 2020.

682 Xu, W., Takeuchi, M., Chen, C., Qiu, Y., Xie, C., Xu, W., Ma, N., Worsnop, D. R., Ng, N. L., and Sun, Y.: Estimation of
683 particulate organic nitrates from thermodenuder–aerosol mass spectrometer measurements in the North China
684 Plain, *Atmos. Meas. Tech.*, 14, 3693–3705, 10.5194/amt-14-3693-2021, 2021.

685 Yang, D., Li, C., Lau, A. K. H., and Li, Y.: Long-term measurement of daytime atmospheric mixing layer height over
686 Hong Kong, *Journal of Geophysical Research*, 118, 2422–2433, 2013.

687 Yang, S., Yuan, B., Peng, Y., Huang, S., Chen, W., Hu, W., Pei, C., Zhou, J., Parrish, D. D., Wang, W., He, X., Cheng, C.,
688 Li, X. B., Yang, X., Song, Y., Wang, H., Qi, J., Wang, B., Wang, C., Wang, C., Wang, Z., Li, T., Zheng, E., Wang, S., Wu,
689 C., Cai, M., Ye, C., Song, W., Cheng, P., Chen, D., Wang, X., Zhang, Z., Wang, X., Zheng, J., and Shao, M.: The
690 formation and mitigation of nitrate pollution: comparison between urban and suburban environments, *Atmos.
691 Chem. Phys.*, 22, 4539–4556, 10.5194/acp-22-4539-2022, 2022.

692 Yao, T., Li, Y., Gao, J., Fung, J. C. H., Wang, S., Li, Y., Chan, C. K., and Lau, A. K. H.: Source apportionment of secondary
693 organic aerosols in the Pearl River Delta region: Contribution from the oxidation of semi-volatile and intermediate
694 volatility primary organic aerosols, *Atmospheric Environment*, 222, 117111, 10.1016/j.atmosenv.2019.117111, 2020.

695 Yu, Y., Cheng, P., Li, H., Yang, W., Han, B., Song, W., Hu, W., Wang, X., Yuan, B., Shao, M., Huang, Z., Li, Z., Zheng, J.,
696 Wang, H., and Yu, X.: Budget of nitrous acid (HONO) at an urban site in the fall season of Guangzhou, China, *Atmos.
697 Chem. Phys.*, 22, 8951–8971, 10.5194/acp-22-8951-2022, 2022.

698 Zhang, Q., Jimenez, J. L., Canagaratna, M. R., Allan, J. D., Coe, H., Ulbrich, I., Alfarra, M. R., Takami, A., Middlebrook,
699 A. M., Sun, Y. L., Dzepina, K., Dunlea, E., Docherty, K., DeCarlo, P. F., Salcedo, D., Onasch, T., Jayne, J. T., Miyoshi, T.,
700 Shimojo, A., Hatakeyama, S., Takegawa, N., Kondo, Y., Schneider, J., Drewnick, F., Borrmann, S., Weimer, S.,
701 Demerjian, K., Williams, P., Bower, K., Bahreini, R., Cottrell, L., Griffin, R. J., Rautiainen, J., Sun, J. Y., Zhang, Y. M., and
702 Worsnop, D. R.: Ubiquity and dominance of oxygenated species in organic aerosols in anthropogenically-influenced
703 Northern Hemisphere midlatitudes, *Geophysical Research Letters*, 34, n/a–n/a, 10.1029/2007GL029979, 2007.

704 Zhang, Q., Jimenez, J. L., Canagaratna, M. R., Ulbrich, I. M., Ng, N. L., Worsnop, D. R., and Sun, Y.: Understanding
705 atmospheric organic aerosols via factor analysis of aerosol mass spectrometry: a review, *Analytical and Bioanalytical*

706 Chemistry, 401, 3045-3067, 10.1007/s00216-011-5355-y, 2011.
707 Zhang, Y. J., Tang, L. L., Wang, Z., Yu, H. X., Sun, Y. L., Liu, D., Qin, W., Canonaco, F., Prevot, A. S. H., Zhang, H. L.,
708 and Zhou, H. C.: Insights into characteristics, sources, and evolution of submicron aerosols during harvest seasons
709 in the Yangtze River delta region, China, *Atmospheric Chemistry and Physics*, 15, 1331-1349, 10.5194/acp-15-
710 1331-2015, 2015.
711 Zhao, J., Qiu, Y., Zhou, W., Xu, W., Wang, J., Zhang, Y., Li, L., Xie, C., Wang, Q., Du, W., Worsnop, D. R., Canagaratna,
712 M. R., Zhou, L., Ge, X., Fu, P., Li, J., Wang, Z., Donahue, N. M., and Sun, Y.: Organic Aerosol Processing During Winter
713 Severe Haze Episodes in Beijing, *Journal of Geophysical Research: Atmospheres*, 124, 10248-10263,
714 10.1029/2019JD030832, 2019.
715 Zhou, W., Xu, W., Kim, H., Zhang, Q., Fu, P., Worsnop, D. R., and Sun, Y.: A review of aerosol chemistry in Asia:
716 insights from aerosol mass spectrometer measurements, *Environmental Science: Processes & Impacts*, 22, 1616-
717 1653, 10.1039/D0EM00212G, 2020.
718